# Enhanced corrosion inhibition of low carbon steel in HCl medium using 1-benzyl-5-imino-3-hydroxypyrazoline: a comprehensive study

**A.W. Saeed,[1] H. Al-Luaiby,[2] A. Mohammed,[3] T.S. Gaaz[4] and A. Alamiery[5]**

[1]*College of Renewable Energy Sciences and Environmental, Alkarkh University of Science, Baghdad 10001, Baghdad, Iraq*
[2]*College of Energy and Environmental Sciences, Al-Karkh University of Science, Baghdad 10001, Baghdad, Iraq*
[3]*Department of Electromechanical Engineering, University of Technology-Iraq, P.O. Box: 10001, Baghdad, Iraq*
[4]*Air Conditioning and Refrigeration Techniques Engineering Department, College of Engineering and Technologies, Al-Mustaqbal University, 51015 Babylon, Iraq*
[5]*Al-Ayen University, Nile St, Nasiriyah, 64001, Dhi Qar, Iraq*
**E-mail: dr.ahmed1975@gmail.com*

## Abstract

This research explores the corrosion inhibition efficiency of 1-benzyl-5-imino-3-hydroxypyrazoline (BIHP) for low carbon steel in hydrochloric acid (HCl) solution. The study assesses BIHP's performance using weight loss measurements, and density functional theory (DFT) calculations. Experimental results demonstrate that BIHP offers an impressive inhibition efficiency of 93% at 303 K during a 5-hour immersion period. Weight loss measurements show a significant decrease in corrosion rates with increasing immersion times (1, 5, 10, 24, and 48 hours), with the inhibition efficiency stabilizing after 10 hours. Furthermore, an increase in inhibition efficiency was demonstrated with increasing temperature from 303 to 333 K. The adsorption of BIHP molecules on the low-carbon steel surface followed the Langmuir model suggesting both physical and chemical adsorption mechanisms. With the help of density functional theory calculations, the most important parameters related to the molecular ability as corrosion inhibitors including the $E_{HOMO}$, $E_{LUMO}$, $E_{gap}$, and issues related to chemical reactions, including total hardness (η), electronegativity (χ), and electron fraction transitions from the anti-corrosion molecule to the low carbon steel ($\Delta N$), were calculated.

Received: November 21, 2024. Published: March 21, 2025 doi: 10.17675/2305-6894-2025-14-1-21

***Keywords:*** *corrosion, hydroxypyrazoline, weight loss, DFT, mechanisms.*

## 1. Introduction

Corrosion of low-carbon steel remains a significant challenge in industries that operate in corrosive environments, particularly in oil and fuel production, chemical processing, and water treatment. Low carbon steel is highly susceptible to corrosion, especially when exposed to HCl, despite its low cost and significant mechanical characteristics [1]. Acidification process involves injecting HCl into the well to dissolve carbonate formations, facilitating fluid flow and increasing well productivity [2]. However, this process also accelerates the corrosion of steel infrastructure, especially in deep wells with high temperatures [3]. Therefore, corrosion inhibitors play an important role in preventing metal damage and ensuring the durability of equipment used in acidification treatments. Corrosion inhibitors are compounds that reduce the corrosion rate and forming a protective barrier between the metal surface and the acidic solution. Natural and/or organic inhibitors, show excellent anticorrosion performance [4]. Among the organic molecules, Imidazoles [5], triazoles [6], tetrazoles [7], and pyridines [8] are considered efficient corrosion inhibitors of metals [9]. Nitrogen-based inhibitors, especially those containing amine, imino, and hydroxyl groups, have shown significant adsorption and exceptional corrosion impedance by forming coordination bonds with the metal surface [10]. Among these, pyrazolines have attracted considerable attention due to their enhanced interactions with metal surfaces, leading to superior corrosion inhibition in corrosive media [11]. Heat exchangers, which are of great importance in petrochemical processing, power generation and water desalination, are highly susceptible to acid-induced corrosion. Corrosion reduces their operational efficiency, increases maintenance costs, and shortens their service life. The use of inhibitors such as BIHP has been shown to enhance corrosion resistance by forming a protective layer on the metal surface, thereby reducing material degradation [12]. The use of such inhibitors in industrial systems ensures sustained performance, reduces maintenance costs, and extends equipment life. Inhibition efficiency is often temperature dependent, and some inhibitors exhibit poor performance at high temperatures due to adsorption from the metal surface, while others maintain or even enhance inhibition efficiency through stronger chemical adsorption [13]. This temperature sensitivity is particularly significant in the oil and gas industry, where extreme downhole temperatures are common [14].

Recently, computational chemistry, as a fast, inexpensive, and reliable tool, has garnered interest in the investigation and evaluation of corrosion inhibitors' performance in different media and metal surfaces. Many documents have been published in the literature dealing with the mechanism and assessment of effective parameters of corrosion inhibitors on a molecular scale [15]. Quantum parameters, such as frontier orbitals (HOMO and LUMO), dipole moment, and electron density distribution, provide insights into the adsorption behavior of corrosion inhibitors [16, 17]. Adsorption models, such as the Langmuir and Temkin isotherms, were used to study the interactions between metal and inhibitors molecules, aiding in the design and application of high-performance corrosion inhibitors [18–20]. Organic inhibitors are particularly valuable in applications where

variable temperature and pressure conditions affect inhibitor performance [21, 22]. In addition, chelating agents and surfactants have been incorporated into corrosion inhibitor formulations to improve adsorption and dissolution properties. Chelating agents such as phosphonates and carboxylate-based inhibitors effectively reduce corrosion rates by forming stable metal-inhibitor complexes [23]. The incorporation of surfactant-based inhibitors has also been explored as a means of enhancing film formation and inhibitor efficiency [24]. These recent developments highlight the need to combine experimental and computational approaches to develop corrosion inhibitors with high efficiency, long-term stability, and environmental sustainability [25]. Corrosion of low carbon steel in HCl solution, is a major challenge in industries. The use of corrosion inhibitors is a widespread approach to mitigate metal degradation, but many conventional inhibitors face limitations related to temperature stability, sorption behavior, and efficiency at higher concentrations. This study explores BIHP (Figure 1) as a potential corrosion inhibitor, and investigates its inhibition performance using weight loss measurements. Unlike previous studies that primarily focus on electrochemical evaluations or newly synthesized compounds, this research provides the first-ever evaluation of BIHP inhibition efficiency using weight loss techniques, focusing on temperature-dependent performance (303 K–333 K) and sorption behavior in acidic media. The Langmuir mode is applied to understand the sorption mechanism of BIHP, while DFT calculations are employed to study the electronic characteristics and interactions between BIHP molecules and the steel surface. The aim of this study is to evaluate the corrosion inhibition efficiency of BIHP through weight loss measurements and computational methods, to demonstrate its feasibility as an effective corrosion inhibitor. The insights gained from this study will contribute to the development of more efficient, thermally stable, and industrially applicable corrosion inhibitors. The main objectives of this study are:

1. To assess the corrosion inhibition efficiency of BIHP for low-carbon steel in HCl solution using weight loss measurements.
2. To evaluate the effect of temperature (303 K–333 K) on the inhibition efficiency of BIHP and determine its thermal stability.
3. To investigate the adsorption behavior of BIHP on the metal surface using Langmuir adsorption isotherm modeling.
4. To perform Density Functional Theory (DFT) calculations to analyze the electronic properties and adsorption interactions of BIHP with the steel surface.
5. To compare the inhibition performance of BIHP with previously studied corrosion inhibitors and assess its potential for industrial applications.

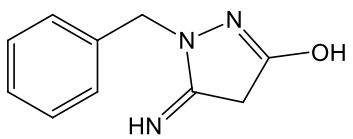


**Figure 1.** BIHP chemical structure.

## 2. Experimental Details

### *2.1. Materials*

In this study, low carbon steel was used with the following chemical composition: 0.21 wt.% carbon (C), 0.005 wt.% manganese (Mn), 0.38 wt.% silicon (Si), 0.05 wt.% sulfur (S), 0.01 wt.% aluminum (Al), 0.09 wt.% phosphorus (P), and the remaining balance being iron (Fe). The corrosion behavior of this steel in a 1 M HCl solution, both with and without varied concentrations of BIHP inhibitor, was studied using rectangular steel samples with dimensions of 4.0 cm×2.5 cm×0.1 cm. Prior to the experiments, the steel samples were polished with various grades of emery paper (400, 600, and 1200 grit) to ensure a smooth surface. After polishing, the samples were washed thoroughly with double-distilled water to remove any debris, followed by rinsing with ethanol. The samples were then dried at room temperature before being weighed to determine their initial dry weight [26].

### *2.2. Preparation of HCl solutions*

Analytical grade HCl (37% purity) was obtained from Merck, Malaysia, and used for the preparation of 1 M HCl solution. This acid was diluted with double-distilled water to achieve the desired concentration. BIHP was then added to the 1 M HCl environment in various concentrations, and the mixture was stirred thoroughly to ensure complete dissolution and uniform distribution of the inhibitor in the solution [27]

### *2.3. Gravimetric analysis*

Weight loss techniques were performed using low carbon steel samples immersed in HCl solution [26, 27]. The metallic samples, each with an exposed surface area of one cm², have been polished and wiped clean to remove any contaminants, ensuring consistency in the results. These samples had been then immersed in glass beakers containing 500 mL of 1 M HCl solution. To compare the overall performance of BIHP as a corrosion inhibitor, its concentration varied from 0.1 mM to 1 mM. The experiments have been performed at different temperatures, ranging from 303 K to 333 K, using a thermostat-controlled water bath to preserve precise temperature control. The metallic samples were removed from the solution after immersion periods of 5, 10, 24, and 48 hours. Each sample was thoroughly washed with ultrapure water and ethanol in an ultrasonic cleanser to remove any corrosion products. The samples were dried and weighed to determine the weight loss [28]. This experimental setup, with the gravimetric method for weight loss measurements, adheres to the standards set with the aid of the National Association of Corrosion Engineers (NACE) for corrosion studies [26, 27]. The following formulas were applied to compute the corrosion rate (*CR*), inhibition efficiency (*IE*%), and surface coverage (θ):

$$CR = \frac{W}{at}, \tag{1}$$

where: $W$ was the weight loss in grams, a was the exposed surface area of the steel sample ($cm^2$), and $t$ was the immersion time (hours).

$$IE\% = \left[1 - \frac{CR_i}{CR_0}\right] \cdot 100, \quad (2)$$

where: $CR_0$ is the corrosion rate without the inhibitor (control), $CR_i$ is the corrosion rate with the inhibitor.

*2.4. Theoretical study*

The quantum chemical calculations of the investigated compounds were performed using the method described in reference [29], implemented *via* the GAMESS application package. The geometric optimization of the molecules was accomplished at the DFT-B3LYP/6–31G(d) level of theory, ensuring that the optimized structures were used for subsequent calculations. Quantum chemical parameters such as $E_{HOMO}$ and $E_{LUMO}$ were computed to gain insight into the electronic properties of the compounds. Koopman's theorem [30] was used to determine the quantum indices, such as ionization potential ($I$), electron affinity ($A$), electronegativity ($\chi$), chemical hardness ($\eta$), and softness ($\sigma$), were calculated regarding equations 3–7:

$$I = -E_{HOMO} \quad (3)$$

$$I = -E_{LUMO} \quad (4)$$

$$\chi = \frac{I + A}{2} \quad (5)$$

$$\eta = \frac{I - A}{2} \quad (6)$$

$$\sigma = \eta^{-1} \quad (7)$$

Additionally, the fraction of electron transfer ($\Delta N$) was calculated using the equation (8):

$$\Delta N = \frac{7 - \chi_{inh}}{2\eta_{inh}}, \quad (8)$$

where $\chi_{inh}$ is the electronegativity of the inhibitor and $\eta_{inh}$ refers to the hardness of the inhibitor, and the reference values for iron were taken as $\chi_{Fe} = 7$ eV and $\eta_{Fe} = 0$ eV.

## 3. Results and Discussion

### *3.1. Gravimetrical measurements*

#### *3.1.1. Effect of inhibitor concentration*

The concentration of BIHP plays an important role in determining its corrosion inhibition ability for low-carbon metal in acid media. Figure 2 shows the relationship between inhibition efficiency (*IE*%) and corrosion rate (*CR*) as a function of BIHP concentration, measured at 303 K over a 5 h exposure period. As seen in Figure 2, the corrosion rate of low carbon steel decreases sharply with increasing BIHP concentration, reaching a plateau at 0.5 mM, where the inhibition efficiency peaks at 93%. This suggests that BIHP exhibits significant inhibition properties by adsorbing on steel surface and forming a protective barrier. The structure of BIHP, which contains aromatic and heterocyclic rings, plays a important role in this process. These structural features enable BIHP to adhere effectively to the steel surface, facilitating the formation of coordination bonds with iron atoms. The interaction strengthens the protective film, making it more resistant to chloride ion penetration. As the concentration of BIHP increases, more inhibitor molecules adsorb onto the metal surface, resulting in the formation of a denser protective layer. This layer acts as a physical barrier that isolates the steel from the aggressive acidic environment, thereby reducing the corrosion rate. At concentrations beyond 0.5 mM, no significant increase in inhibition efficiency was observed, suggesting that the metal surface has reached saturation with BIHP adsorption [31]. This behavior was consistent with other studies that have shown a saturation point at which the protective effect of the inhibitor no longer increases with concentration. It was also important to note that while increasing the concentration of corrosion inhibitors generally enhances protection, excessively high concentrations could lead to adverse effects. In some cases, excessive inhibitor concentration could disrupt the uniformity of the protective film or cause the desorption of inhibitor molecules, resulting in increased corrosion rates. However, in the case of BIHP, the optimal concentration for maximum inhibition efficiency was determined to be 0.5 mM, beyond which no further improvement was observed. Figure 2 shows a sharp decrease in the corrosion rate as the BIHP concentration increases, with the most significant reduction occurring between 0 and 0.1 mM. The corrosion rate decreases gradually until it stabilizes at 0.4 mM, indicating that the protective film formed by BIHP molecules has reached full coverage of the steel surface. At this point, the corrosion rate reached its lowest value, and further increases in BIHP concentration do not result in additional protection. The red curve in Figure 2 illustrates the inhibition efficiency (*IE*%), which increases with inhibitor concentration, reaching a maximum of 93% at 0.5 mM. This behavior indicates that BIHP effectively inhibits corrosion by forming a stable protective layer on the metal surface. The plateau in the inhibition efficiency curve indicates metal surface saturation, and the addition of more BIHP molecules does not enhance protection beyond this point.

Previous studies support these findings. For example, Mitra *et al.* [32] conducted tests using organic inhibitors in 1 M HCl solution and found that higher inhibitor concentrations generally reduced the corrosion rate. However, the optimal concentration varied depending on the specific inhibitor used. Similarly, Kumar *et al.* [33] observed that pomegranate peel extract had a maximum inhibition efficiency at a specific concentration, beyond which no further improvement was achieved. Olasunkanmi also found that the use of castor oil as an eco-friendly inhibitor in HCl solution led to a decrease in corrosion rates until a certain concentration, beyond which inhibition efficiency declined. In conclusion, BIHP exhibits excellent performance as a corrosion inhibitor for low carbon steel in acidic environments. Its adsorption onto the steel surface forms a stable and protective film, reducing the corrosion rate significantly. The optimal concentration for maximum inhibition efficiency was 0.5 mM, beyond which no further improvement was observed. These findings highlight the potential of BIHP as a reliable corrosion inhibitor in industrial applications where acidic media pose a significant risk to steel infrastructure.

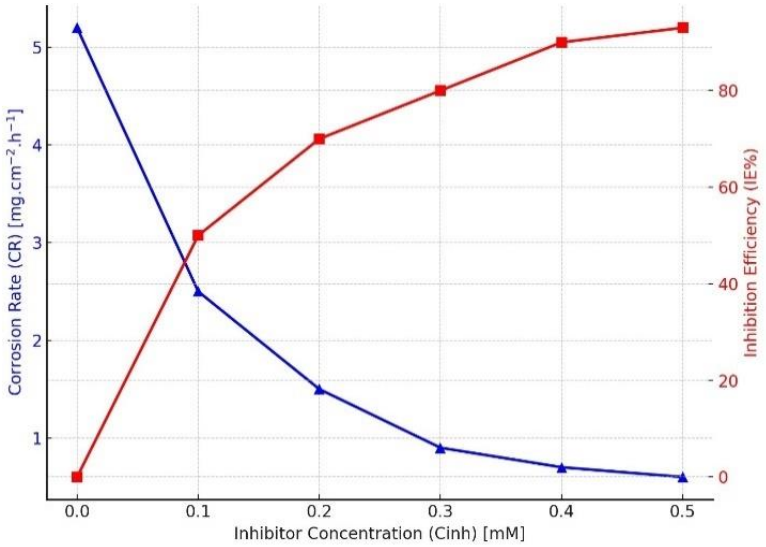


**Figure 2.** Effect of BIHP concentration on corrosion rate (*CR*) and inhibition efficiency (*IE*%) for low carbon steel in 1 M HCl solution at 303 K.

### *3.1.2. Effect of immersion time*

To assess the effect of exposure time on BIHP's corrosion inhibition performance, low carbon steel was immersed in 1 M HCl solution with different BIHP concentrations (0.1 to 1.0 mmol) for different time periods, ranging from 1 to 48 h, at 303 K. Figure 3 shows the relationship between corrosion rate and inhibition efficiency as a function of BIHP concentration and exposure time. The experimental findings show a significant decrease in the corrosion rate with increasing BIHP concentrations and extended immersion periods, and also the corrosion rate decreased by approximately 40% because as the BIHP concentration increased from 0.1 mM to 0.5 mM. At 1.0 mM BIHP, the corrosion rate showed a greater

decrease compared to the 0.1 mmol concentration, demonstrating the effectiveness of BIHP as a corrosion inhibitor over extended time periods.

Furthermore, longer exposure periods were found to enhance the inhibition efficiency, especially up to 24 h. After 24 h, the inhibition performance stabilized, indicating that the BIHP molecules had fully interacted with the steel surface, forming a strong protective layer. This persistent behavior after 24 h was attributed to the saturation of adsorption sites on the steel surface, limiting further improvement in corrosion protection after this period. Increased immersion periods allowed for the development of a more protective layer, enhancing the stability and corrosion inhibition capabilities of BIHP. However, the depletion of available BIHP molecules due to their reaction with the metal surface leads to a stabilization of inhibition efficiency after prolonged exposure. This shows that extra factors, such as solution temperature or pH, may influence the overall efficiency of BIHP at prolonged time intervals. The mechanism behind BIHP's inhibitory action was likely due to its ability to form strong hydrogen bonds and coordination interactions with the steel surface. These interactions improve the stability of the protective layer and enhance its ability to prevent or reduce corrosion. Its enhanced corrosion prevention is attributed dual adsorption mechanisms, involving both physisorption and chemisorption, which collectively form a dense and compact film. This film acts as a strong barrier, protecting the metal from corrosive agents [34]

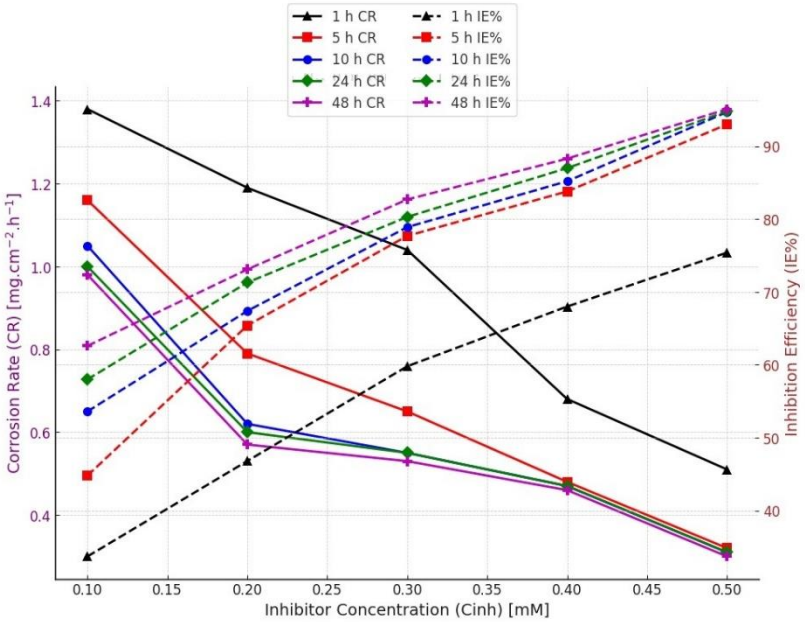


**Figure 3.** Effect of BIHP concentration and immersion time on corrosion rate and inhibition efficiency.

### *3.1.3. Effect of temperature*

This study investigated the impact of temperature on the corrosion inhibition efficiency of BIHP for low-carbon steel. Figure 4 illustrates how the corrosion rate and inhibition

performance of BIHP change with temperature, ranging from 303 K to 333 K. The results clearly show that the corrosion rate of low-carbon steel decreases as the temperature increases, while the inhibition efficiency of BIHP slightly improves at higher temperatures [35].

At all tested concentrations, BIHP maintained its corrosion inhibitory efficiency across the entire temperature range, with the inhibition efficiency showing a slight increase as the temperature was raised from 303 K to 333 K. This temperature-dependent behavior highlights the strong interaction between BIHP and the metal surface, which is enhanced by physical and chemical adsorption mechanisms. For example, at a concentration of 0.5 mmol, BIHP demonstrated superior performance at 303 K, and its overall performance improved slightly as the temperature was increased to 333 K. This indicates that BIHP can effectively protect low-carbon steel from corrosion in acidic environments, even at high temperatures. The increased temperature enhances the interaction between the inhibitor molecules and the steel surface, promoting better surface coverage and more efficient corrosion protection.

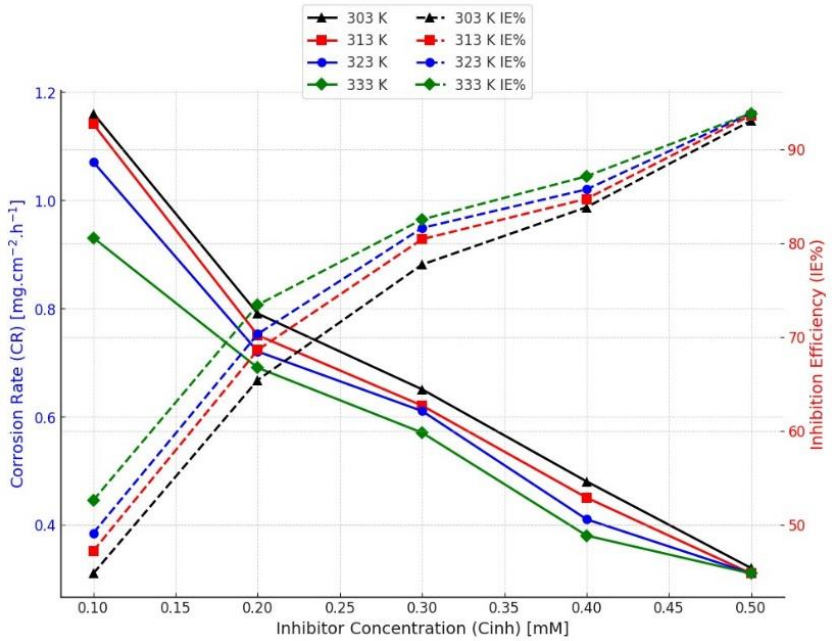


**Figure 4.** Effect of temperature on BIHP inhibition efficiency and corrosion rate.

### *3.2. Adsorption isotherm*

The adsorption behavior of BIHP on the low carbon steel surface became analyzed using several adsorption isotherms, including Langmuir, Temkin, and Freundlich patterns [36]. The Langmuir model was found to be the most suitable isotherm to demonstrate the adsorption of BIHP on the steel surface. Langmuir model indicates that the adsorption occurs as a monolayer, with a uniform distribution of active sites on the steel surface, where each site can accommodate only one inhibitor molecule. The degree of surface coverage (θ) was calculated based on weight loss measurements using the relation $\theta = (W_0 - W_i)/W_0$, where $W_0$ and $W_i$ represent the weight loss in the absence and presence of the inhibitor, respectively.

This approach assumes that the inhibitor predominantly functions *via* a blocking mechanism, where adsorbed molecules prevent direct contact between the metal surface and the corrosive environment. While this method provides a practical estimation of surface coverage, it is acknowledged that it may not fully capture complex adsorption phenomena, such as multilayer formation or chemical bonding interactions. The adsorption behavior following the Langmuir isotherm supports the assumption of monolayer coverage and the direct correlation between inhibition efficiency and surface coverage. As shown in Figure 5, the linear plot of $C_{inh}/\theta$ *versus* $C_{inh}$, demonstrates that the adsorption of BIHP follows the Langmuir model, with the calculated slope and intercept values being 0.889 and 0.0781, respectively. In this case, the high correlation coefficient ($R^2 = 0.99508$) confirms the applicability of the Langmuir model.

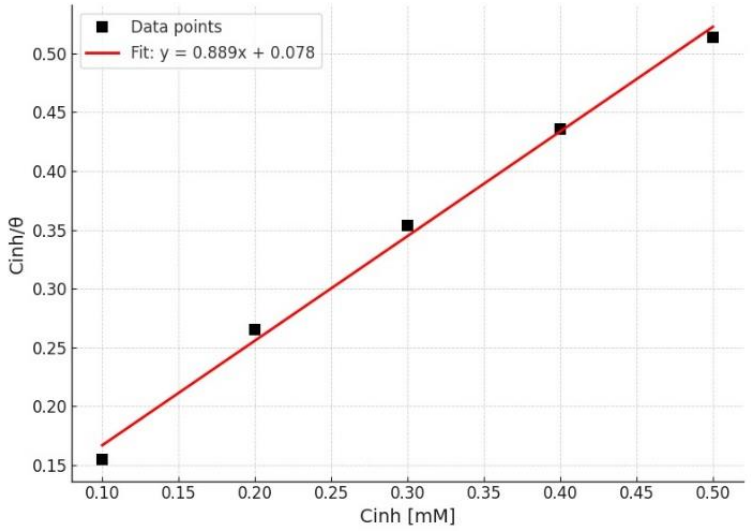


**Figure 5.** Langmuir adsorption isotherm for BIHP on low carbon steel.

The Temkin model indicates that the initial interaction between BIHP molecules and the metal surface is strong but weakens as surface coverage increases. Additionally, the Freundlich model was applied to evaluate surface heterogeneity and the possibility of multilayer adsorption. This isotherm assumes that the surface of the metal was heterogeneous, and the adsorption sites vary in strength. Although the adsorption of BIHP predominantly followed the Langmuir model, the Freundlich isotherm suggests the potential for multilayer adsorption, further supporting the coexistence of physisorption and chemisorption. The Langmuir adsorption parameters, including the equilibrium constant $K_{ads}$, were calculated based on the linear plot in Figure 5. The equation used for this calculation is given by:

$$\frac{C}{\theta} = \frac{1}{K_{ads}} + C, \tag{9}$$

where $C$ is the inhibitor concentration, and θ represents surface coverage [37], and $K_{ads}$ was the adsorption equilibrium constant.

The Gibbs free energy of adsorption $\Delta G_{ads}^{0}$ was determined using the equation:

$$\Delta G_{ads}^{0} = -RT \ln(55.5 K_{ads}), \quad (10)$$

where $R$ is the universal gas constant, $T$ is the absolute temperature (K), and 55.5 is the molar concentration of water in the solution.

The calculated $\Delta G_{ads}^{0}$ value for BIHP was −35.73 kJ/mol, indicating that the adsorption process is spontaneous and involves both chemisorption and physisorption. A $\Delta G_{ads}^{0}$ value close to −40 kJ/mol suggests that chemisorption is dominant, while physical adsorption also plays a role. This combination of adsorption mechanisms facilitates the formation of a stable protective film on the metal surface. The adsorption of BIHP on the low carbon steel surface involves a combination of physical and chemical interactions. The Langmuir isotherm provides the best fit for the experimental data, indicating monolayer adsorption of BIHP molecules. However, the Temkin and Freundlich isotherms [38] provide additional insights, indicating that physisorption and chemisorption coexist, contributing to a spontaneous and stable adsorption process. This dual adsorption mechanism enhances the corrosion inhibition efficiency of BIHP, making it a promising candidate for use in acidic environments.

### *3.3. Quantum chemical calculations*

Quantum chemical calculations provide vital insights into the electronic structure and reactivity of corrosion inhibitors. In this study, DFT using the B3LYP hybrid functional method was employed to analyze the corrosion inhibition efficiency of BIHP. Figure 6 shows the geometry of optimized structure and electron density distribution of the frontier molecular orbitals (FMO), whereas Table 1 demonstrates the theoretical characters obtained for the BIHP molecules, such as $E_{HOMO}$, $E_{LUMO}$, the energy gap ($\Delta E_{gap}$), and other related factors.

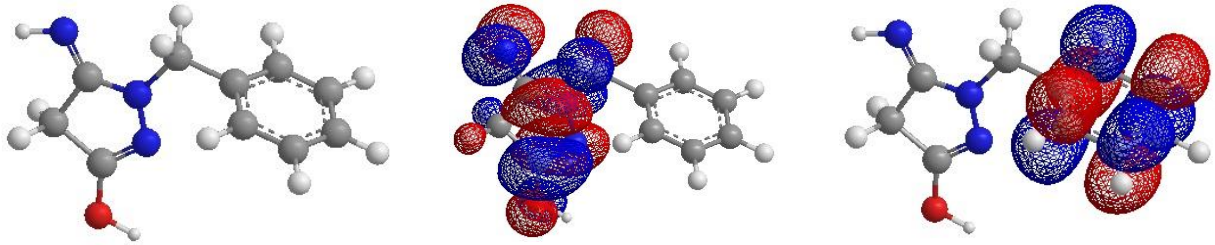

Optimized Structure HOMO LUMO

**Figure 6.** Optimized structure, HOMO, and LUMO of BIHP.

The optimized geometry of the BIHP molecule clearly shows its almost planar structure, which was crucial for its effective adsorption onto the steel surface. The inclusion of various functional groups, such as the imino and hydroxyl organizations, enhances the molecule's ability to interact with the metallic surface through electron-donating effects. The

molecular planarity provides a large surface area for adsorption, which promotes better corrosion inhibition. As seen from the HOMO and LUMO distributions in Figures 6a and 6b, the electron density inside the HOMO was primarily concentrated on the diazole ring and functional groups, such as the imino and hydroxyl groups. This indicates that these regions were primarily responsible for donating electrons to the steel surface. In comparison, the LUMO was mainly localized on the benzene ring, indicating that this part of the molecule was more likely to accept electrons from the steel.

The electron density distribution across the HOMO and LUMO orbitals suggests a dual interaction among the BIHP molecules and the low carbon metallic surface. The HOMO was involved in donating electrons to the steel surface, while the LUMO accepts electrons from the metal's *d*-orbitals. This interplay strengthens the adsorption of the inhibitor on the metal surface. Several quantum chemical parameters were calculated using DFT, as shown in Table 1. These parameters, which includes $E_{HOMO}$, $E_{LUMO}$, and $\Delta E_{gap}$, provide insights into the electronic properties of the inhibitor and its effectiveness in corrosion inhibition. The optimized structure of BIHP indicates its nearly planar conformation, which allows for huge surface coverage at the metallic substrate. The purposeful companies, particularly the imino and hydroxyl businesses, play a crucial role in electron donation and interplay with the steel surface. This planarity guarantees that the molecule can establish strong interactions with the metal surface, enhancing its corrosion inhibition performance [39]. HOMO plot demonstrates the areas of the molecule where electron density was most likely to donate electrons. In the case of BIHP, the HOMO was in most cases localized across the diazole ring and the practical agencies, indicating these regions had been liable for electron donation to the metal surface. This strong electron-donating capacity enhances the chemisorption of BIHP onto the metal surface, forming a stable protecting layer. LUMO was primarily concentrated on the benzene ring of the molecule. The LUMO represents the regions of the molecule most likely to accept electron from the metal surface. The distribution of the LUMO indicates that BIHP can also accept electrons from the d-orbitals of the metal atoms, in addition strengthening the adsorption procedure and making the inhibitor more effective in preventing corrosion. Total hardness (η) and global softness (σ) reveal the stability and reactivity. Hardness with law value refers to higher reactivity, whereas softness with greater signifies stronger adsorption potential. The tested inhibitor, has low hardness value and high softness value which indicate strong adsorption ability and enhanced corrosion inhibition. Additionally, $\Delta N$ confirms BIHP's ability to donate electrons to the Fe atom, further reinforcing its protective effect [40]. These findings align with the experimental outcomes, assisting the effectiveness of BIHP as a corrosion inhibitor.

**Table 1.** Quantum chemical parameters of BIHP.

| $I$ (eV) | $A$ (eV) | $E_{HOMO}$ (eV) | $E_{LUMO}$ (eV) | $\Delta E_{gap}$ (eV) | χ (eV) | η (eV) | σ ($eV^{-1}$) | $\Delta N$ |
|---|---|---|---|---|---|---|---|---|
| –7.543 | 0.375 | –7.543 | 0.375 | 7.918 | 3.584 | 3.959 | 0.253 | 0.182 |

The values provided in Table 1 are key indicators of the reactivity, balance, and electron-donating/accepting conduct of the BIHP molecule as a corrosion inhibitor.

$E_{HOMO}$ (−7.543 eV) fee represents the ionization potential of BIHP. A higher $E_{HOMO}$ value indicates a strong ability to donate electrons to the metal surface. In this situation, the noticeably high $E_{HOMO}$ indicates that BIHP has a strong tendency to donate electrons, which aids in forming a protective layer on the metal, improving its inhibitory performance. $E_{LUMO}$ (0.375 eV) value represents the electron affinity of the molecule, which determines its ability to just accept electrons from the steel surface. The low $E_{LUMO}$ value indicates that BIHP ought to effectively receive electrons, allowing strong interaction with the metal surface and further enhancing its adsorption properties. Using HOMO and LUMO energies and calculating the gap energy, the chemical reactivity of molecules with the metal surface could be determined. A decrease in energy gap, the capability of the molecule to form bonds with the metal surface increases. In this case, the energy gap of 7.918 eV suggests that BIHP is moderately reactive and can effectively interact with the steel surface. Electronegativity represents the ability of a molecule to attract electrons. A moderate $\chi$ value indicates that BIHP can balance electron donation and acceptance, a property that promotes its adsorption onto the metal surface through chemical and physical interactions. Global hardness ($\eta = 3.959$ eV) and global softness ($\sigma = 0.253$ eV$^{-1}$) were measures of molecular stability and reactivity. Lower hardness and better softness values are associated with better adsorption and reactivity. BIHP's values suggest that it is highly soft and reactive, allowing it to form strong interactions with the metal surface. The positive value of $\Delta N$ ($\Delta N = 0.182$) suggests that BIHP donates electrons to the metal surface, facilitating the formation of a strong protective film. This electron transfer is key to its inhibition efficiency, as it allows sturdy bonding with the steel substrate.

The quantum chemical calculations reveal that BIHP has excellent properties for corrosion inhibition. Its high $E_{HOMO}$ value demonstrates strong electron-donating ability, while the low $E_{LUMO}$ value suggests significant electron-accepting capacity, whilst the low $E_{LUMO}$ value indicates true electron-accepting ability. $\Delta E_{gap}$ highlights its reactivity, and the advantageous electron transfer ($\Delta N$) confirms its sturdy interplay with the metal surface. Together, those elements make a contribution to BIHP's high inhibition efficiency, as observed in each the experimental and theoretical studies. The HOMO and LUMO density distributions, mixed with the quantum chemical parameters, offer a understanding expertise of ways BIHP interacts with the metal surface, making it an effective inhibitor for corrosion prevention in acidic environments [41].

The Mulliken charge analysis provides insights into the electron distribution inside the BIHP molecule, which helps identify potential sites for adsorption on the metal surface. In the context of corrosion inhibition atoms with negative charges are more likely to interact with the positively charged metallic surface, leading to stronger adsorption and improved corrosion protection. From Figure 7 shows that specific atoms in the BIHP molecule possess significantly negative charges, such as nitrogen and oxygen atoms [42]. These atoms, with higher electron density, serve as the primary sites for interaction with the metal surface. The

negative charges on these atoms increase their ability to donate electrons, thus facilitating chemisorption onto the metal surface

Nitrogen atoms (N1, N2, N7) in the molecule exhibit significant variations in their Mulliken charges. Notably, N7 (imine nitrogen) has a highly negative charge (–0.749), making it a key site for interaction with the metal surface. Similarly, N2 (imine nitrogen) possesses a moderately negative charge (−0.248). These negatively charged nitrogen atoms were likely to coordinate with the positively charged metal atoms, thereby enhancing adsorption through chemisorption. Oxygen atom (O6) in the enol group exhibits a negative charge of −0.292. This suggests that the oxygen atom could also act as a strong electron donor, forming coordination bonds with the metal surface. This further strengthens the protective layer formed by the BIHP molecule on the metal, preventing corrosion. The carbon atoms exhibit varied Mulliken charges. Some carbon atoms, such as C(4) and C(8), have slightly negative charges, while others were more neutral or slightly positive. These carbon atoms likely play a secondary role in adsorption, compared to the more strongly negative nitrogen and oxygen atoms. The Mulliken charge analysis, as shown in Figure 7, indicates that the nitrogen and oxygen atoms in BIHP were the key adsorption sites due to their negative charges. These atoms should donate electrons to the metal surface, facilitating strong chemisorption interactions. The presence of both nitrogen and oxygen atoms in the molecular structure complements the general adsorption functionality of BIHP, making it an effective corrosion inhibitor. The distribution of charges throughout the molecule supports a dual adsorption mechanism, involving each physical and chemical interactions with the metallic surface.

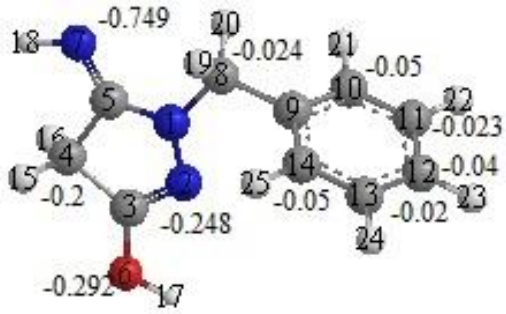


**Figure 7.** Mulliken charge analysis of BIHP.

### *3.4. Suggested inhibition mechanism*

The inhibition of low-carbon steel corrosion in HCl solution by BIHP can be understood through adsorption behavior and molecular interactions, as determined by weight loss measurements and quantum chemical calculations. The inhibition efficiency of BIHP is primarily attributed to its ability to adsorb onto the metal surface, reducing the rate of metal dissolution in an acidic environment. The following steps outline the proposed inhibition mechanism [43–46]:

### *3.4.1. Adsorption of BIHP on the metal surface*

The corrosion inhibition process occurs through adsorption, where BIHP molecules interact with the steel surface, reducing the exposed area susceptible to acid attack. The Langmuir adsorption isotherm, which best fits the experimental data, suggests monolayer adsorption, with each inhibitor molecule occupying a distinct site on the steel surface. The adsorption of BIHP is facilitated by:

- Functional groups within the BIHP molecule, such as imino (–N=), hydroxyl (–OH), and aromatic rings, which serve as active adsorption sites.
- Physisorption due to van der Waals forces between the delocalized π-electrons of the aromatic rings and the metal surface.
- Chemisorption *via* donation of lone pair electrons from nitrogen and oxygen atoms to vacant d-orbitals of iron atoms, forming coordination bonds.

The weight loss data and adsorption isotherm studies indicate that both physisorption and chemisorption contribute to inhibition efficiency, with adsorption strength increasing at lower temperatures.

### *3.4.2. Formation of a surface barrier layer*

Once adsorbed onto the metal, BIHP molecules form a thin monolayer that reduces direct contact between the steel surface and corrosive species ($H^+$ and $Cl^-$ ions)**.** This adsorbed layer does not represent a physically visible protective film but acts as a molecular-level barrier, minimizing acid-induced dissolution.

### *3.4.3. Role of quantum chemical parameters in adsorption*

Density Functional Theory (DFT) calculations provide further insight into the interaction between BIHP and the steel surface:

- The high $E_{HOMO}$ value of BIHP suggests strong electron-donating ability, facilitating chemisorption by donating electrons to the steel surface.
- The low $E_{LUMO}$ value enables BIHP to accept electrons from the metal, strengthening adsorption interactions.
- The relatively small energy gap indicates that BIHP has high reactivity and can readily interact with the steel surface.
- The HOMO density localized around the nitrogen and oxygen sites suggests that these atoms play a key role in adsorption.

### *3.4.4. Temperature dependence of the inhibition mechanism*

The weight loss measurements at different temperatures indicate that BIHP adsorption is spontaneous and exothermic, as evidenced by the calculated negative Gibbs free energy values. At higher temperatures, the decrease in inhibition efficiency suggests partial desorption, reinforcing the physisorption contribution to the adsorption mechanism.

## 4. Conclusion

This study investigated the corrosion inhibition efficiency of BIHP for low-carbon steel in HCl solution using weight loss measurements and quantum chemical calculations. The experimental findings demonstrated that BIHP effectively reduced the corrosion rate of low-carbon steel, achieving a maximum inhibition efficiency of 93% at 303 K for a 5-hour immersion period. The corrosion rate decreased with increasing BIHP concentration, confirming the strong inhibitory effect of the BIHP. Moreover, BIHP maintained a constant inhibition efficiency over extended immersion times, indicating its stable protective behavior under acidic conditions. The adsorption of BIHP on the steel surface followed the Langmuir adsorption curve, confirming the monolayer adsorption. Thermodynamic parameters indicated that the adsorption process was spontaneous and involved a combination of physical and chemical adsorption mechanisms. The inhibition efficiency decreased slightly at higher temperatures, indicating that the adsorption was partially reversible. DFT provided further insight into the electronic properties of BIHP. The high $E_{HOMO}$ value and small energy gap indicate a strong ability to donate electrons, facilitating effective interaction with the low carbon steel surface. Mulliken charge confirmed that nitrogen and oxygen atoms in BIHP molecule served as the primary adsorption sites, forming strong interactions with the low carbon steel surface.

## References

1. J. Du, K. Xiang, L.Q. Zhao, X.T. Lan, P.L. Liu and Y. Liu, Corrosion inhibition of 13Cr stainless steel in HCl/HAc/HF acid solution, *Int. J. Electrochem. Sci*., 2019, **14**, 8919–8930. doi: 10.20964/2019.09.44
2. V.C. Anadebe, P.C. Nnaji, O.D. Onukwuli, N.A. Okafor, F.E. Abeng, V.I. Chukwuike, C.C. Okoye, I.I. Udoh, M.A. Chidiebere, L. Guo and R. Barik, Multidimensional insight into the corrosion inhibition of salbutamol drug molecule on mild steel in oilfield acidizing fluid: Experimental and computer-aided modeling approach, *J. Mol. Liq*., 2022, **349**, 118482. doi: 10.1016/j.molliq.2022.118482
3. S.A. Umoren, M.M. Solomon and V.S. Saji, *Corrosion Inhibitors in the Oil and Gas Industry*, 1st ed., Oxford, UK: Elsevier, 2020, pp. 229–254.
4. C.A. de Wolf, H.A. Nasr-El-Din, A. Bouwman, E.R.A. Bang and E. Naylor, Corrosion rates of Cr- and Ni-based alloys with organic acids and chelating agents used in stimulation of deep wells, *SPE Prod. Oper*., 2017, **32**, 208–202. doi: 10.2118/152716-PA
5. I. Gomaa, M. Mahmoud and M.S. Kamal, Sandstone acidizing using a low-reaction acid system, *J. Energy Resour. Technol*., 2020, **142**, 103008. doi: 10.1115/1.4047317
6. Z. Tariq, A. Hassan, R. Al-Abdrabalnabi, M. Aljawad and M. Mahmoud, Comparative study of fracture conductivity in various carbonate rocks treated with GLDA chelating agent and HCl acid, *Energy Fuels*, 2021, **35**, 19641–19654. doi: 10.1021/acs.energyfuels.1c03471

7. J. Wang, Y.X. Huang, F.J. Zhou, Z.Y. Song and X.Y. Liang, Study on reservoir damage during acidizing for high-temperature and ultra-deep tight sandstone, *J. Pet. Sci. Eng*., 2020, **191**, 107231. doi: 10.1016/j.petrol.2020.107231
8. Y. Shi, L. Yu, S. Chen, Y. He, X. Yang, L. Duan and J. Cai, Effects of L-glutamic acid, N,N-diacetic acid as chelating agent on acidification of carbonate reservoirs in acidic environments, *J. Nat. Gas Sci. Eng*., 2020, **82**, 103494. doi: 10.1016/j.jngse.2020.103494
9. M. Al Hamad, S.A. Al-Sobhi, A.T. Onawole, I.A. Hussein and M. Khraisheh, Density-functional theory investigation of barite scale inhibition using phosphonate and carboxyl-based inhibitors, *ACS Omega*, 2020, **5**, 33323–33328. doi: 10.1021/acsomega.0c05125
10. T. Rabizadeh, C.L. Peacock and L.G. Benning, Investigating the effectiveness of phosphonate additives in hindering the calcium sulfate dihydrate scale formation, *Ind. Eng. Chem. Res*., 2020, **59**, 14970–14980. doi: 10.1021/acs.iecr.0c03600
11. Y. Qiang, L. Guo, H. Li and X. Lan, Fabrication of environmentally friendly losartan potassium film for corrosion inhibition of mild steel in HCl medium, *Chem. Eng. J*., 2021, **406**, 126863. doi: 10.1016/j.cej.2020.126863
12. C. Pragathiswaran, P. Ramadevi and K. Kumar, Imidazole and $Al^{3+}$ nano material as corrosion inhibitor for mild steel in hydrochloric acid solutions, *Mater. Today: Proc*., 2021, **37**, 2912–2916. doi: 10.1016/j.matpr.2020.08.671
13. Y.J. Qiang, H. Zhi, L. Guo, A. Fu, T. Xiang and Y. Jin, Experimental and molecular modeling studies of multi-active tetrazole derivative bearing sulfur linker for protecting steel from corrosion, *J. Mol. Liq*., 2021, **351**, 118638. doi: 10.1016/j.molliq.2022.118638
14. M.L. Hrimla, L. Bahsis, A. Boutouil, M.R. Laamari, M. Julve and S. Stiriba, Corrosion inhibition performance of a structurally well-defined 1,2,3-triazole derivative on mild steel-hydrochloric acid interface, *J. Mol. Struct*., 2021, **1231**, 129895. doi: 10.1016/j.molstruc.2021.129895
15. H.M. Abd El-Lateef, M.M. Khalaf, K. Shalabi and A.A. Abdelhamid, Efficient synthesis of 6,7-dihydro-5*H*-cyclopenta[b]pyridine-3-carbonitrile compounds and their applicability as inhibitor films for steel alloy corrosion, *ACS Omega*, 2022, **7**, 24727–24745. doi: 10.1021/acsomega.2c02639
16. H. Fakhry, M.E. El Faydy, F. Benhiba, T. Laabaissi and M. Allali, A newly synthesized quinoline derivative as corrosion inhibitor for mild steel in molar acid medium, *Colloids Surf. A*, 2021, **610**, 125746. doi: 10.1016/j.colsurfa.2020.125746
17. G. Yerlikaya, A. Ahmad, M. Farsak, H.K. Kilig, G. Kardas and S. Kaya, Illuminating of mild steel/HCl interface in the presence of 5-DAT inhibitor, *J. Mol. Liq*., 2021, **326**, 115380. doi: 10.1016/j.molliq.2021.115380
18. A.O. Ayeni, O.F. Akinyele, E.C. Hosten, E.G. Fakola, J.T. Olalere, G.O. Egharevba and G.M. Watkins, Synthesis, crystal structure, experimental and theoretical studies of corrosion inhibition of a Mannich base, *J. Mol. Struct*., 2020, **1219**, 128539. doi: 10.1016/j.molstruc.2020.128539

19. A.S. El-Tabei, M.A. Hegazy, A.H. Bedair and N.M. El Basiony, Novel macrocyclic cationic surfactants: Synthesis and corrosion inhibition activity for carbon steel, *J. Mol. Liq.*, 2021, **324**, 116990. doi: 10.1016/j.molliq.2021.116990
20. S. Al-Baghdadi, A. Al-Amiery, T. Gaaz and A. Kadhum, Terephthalohydrazide and isophthalo-hydrazide as new corrosion inhibitors for mild steel in hydrochloric acid: Experimental and theoretical approaches, *Koroze Ochr. Mater.*, 2021, **65**, 12–22. doi: 10.2478/kom-2021-0002
21. G. Gece, The use of quantum chemical methods in corrosion inhibitor studies, *Corros. Sci.*, 2008, **50**, no. 11, 2981–2992. doi: 10.1016/j.corsci.2008.08.043
22. B.S. Mahdi, M.K. Abbass, M.K. Mohsin, W.K. Al-Azzawi, M.M. Hanoon, M.H.H. AlKaabi, L.M. Shaker, A.A. Al-Amiery, W.N.R.W. Isahak, A.A.H. Kadhum and M.S. Takriff, Corrosion inhibition of mild steel in hydrochloric acid environment using terephthaldehyde based on Schiff base: Gravimetric, thermodynamic, and computational studies, *Molecules*, 2022, **27**, no. 15, 4857. doi: 10.3390/molecules27154857
23. M. Finšgar and J. Jackson, Application of corrosion inhibitors for steels in acidic media for the oil and gas industry: A review, *Corros. Sci.*, 2014, 86, 17–41. doi: 10.1016/j.corsci.2014.04.044
24. V.M. Abbasov, L.I. Aliyeva, H.M. Abd El-Lateef and I.T. Ismayilov, Some surfactants based on the vegetable oils as $CO_2$ corrosion inhibitors for mild steel in oilfield formation water, *Int. J. Corros. Scale Inhib.*, 2015, **4**, no. 2, 162–175. doi: 10.17675/2305-6894-2015-4-2-162-175
25. Ya.G. Avdeev and Yu.I. Kuznetsov, Acid corrosion of metals and its inhibition: A critical review of the current problem state, *Int. J. Corros. Scale Inhib.*, 2022, **11**, no. 1, 111–141. doi: 10.17675/2305-6894-2022-11-1-6
26. TM0169/G31-12a, Standard Guide for Laboratory Immersion Corrosion Testing of Metals, NACE International, Houston, TX, USA, 2012.
27. ASTM G 31-72, Standard Guide for Laboratory Immersion Corrosion Testing of Metals, American Society for Testing and Materials, Philadelphia, PA, USA, 1990.
28. T.O. Olomola, S. Durodola, L.O. Olasunkanmi and A. Adekunle, Effect of selected 3-chloromethylcoumarin derivatives on mild steel corrosion in acidic medium: experimental and computational studies Effect of selected 3-chloromethylcoumarin derivatives on mild steel corrosion in acidic medium: experimental and computational studies, *J. Adhes. Sci. Technol.*, 2022, **36**, no. 4, 2547–2561. doi: 10.1080/01694243.2022.2094147
29. M.M. Hanoon, A.M. Resen, L.M. Shaker, A.A.H. Kadhum and A.A. Al-Amiery, Corrosion investigation of mild steel in aqueous hydrochloric acid environment using N-(naphthalen-1-yl)-1-(4-pyridinyl)methanimine complemented with antibacterial studies, *Biointerface Res. Appl. Chem.*, 2021, **11**, no. 2, 9735–9743. doi: 10.33263/BRIAC112.97359743

30. T. Koopmans, Ordering of wave functions and eigen-energies to the individual electrons of an atom, *Physica*, 1934, **1**, no. 1–6, 104–113 (in German). doi: 10.1016/S0031-8914(34)90011-2
31. A. Alamiery, W.N.R.W. Isahak, H. Aljibori, H. Al-Asadi and A. Kadhum, Effect of the structure, immersion time and temperature on the corrosion inhibition of 4-pyrrol-1-yl-*N*-(2,5-dimethyl-pyrrol-1-yl)benzoylamine in 1.0 M HCl solution, *Int. J. Corros. Scale Inhib*., 2021, **10**, no. 2, 700–713. doi: 10.17675/2305-6894-2021-10-2-14
32. R.K. Mitra, R. Yadav, A. Tomar and M. Yadav, Computational and experimental evaluation on pyrazoles as corrosion inhibitor in HCl solution: DFT and electrochemical analysis, *Int. J. Corros. Scale Inhib*., 2024, **13**, no. 4, 1908–1935. doi: 10.17675/2305-6894-2024-13-4-2
33. N. Kumar, D. Daniloski, N. Pratibha, N.N. D'Cunha, N. Naumovski and A.T. Petkoska, Pomegranate peel extract – a natural bioactive addition to novel active edible packaging, *Food Res. Int*., 2022, **156**, 111378. doi: 10.1016/j.foodres.2022.111378
34. A.Y. Rubaye, A.A. Abdulwahid, S.B. Al-Baghdadi, A.A. Al-Amiery, A.A. Kadhum and A.B. Mohamad, Cheery sticks plant extract as a green corrosion inhibitor complemented with LC-EIS/MS spectroscopy, *Int. J. Electrochem. Sci*., 2015, **10**, no. 10, 8200–8209. doi: 10.1016/S1452-3981(23)11087-X
35. T.A. Salman, A.A. Al-Amiery, L.M. Shaker, A.A.H. Kadhum and M.S. Takriff, A study on the inhibition of mild steel corrosion in hydrochloric acid environment by 4-methyl-2-(pyridin-3-yl)thiazole-5-carbohydrazide, *Int. J. Corros. Scale Inhib*., 2019, **8**, no. 4, 1035–1059. doi: 10.17675/2305-6894-2019-8-4-14
36. A. Al-Amiery, Anti-Corrosion Performance Of 2-Isonicotinoyl-N-Phenylhydrazinecarbothioamide For Mild Steel Hydrochloric Acid Solution: Insights From Experimental Measurements And Quantum Chemical Calculations, *Surf. Rev. Lett*., 2021, **28**, no. 3, 2050058. doi: 10.1142/S0218625X20500584
37. Yu.I. Kuznetsov, N.N. Andreev and S.S. Vesely, Why we reject papers with calculations of inhibitor adsorption based on data on protective effects, *Int. J. Corros. Scale Inhib*., 2015, **4**, no. 2, 108–109
38. M.D. Plotnikova, M.G. Shcherban, A.B. Shein, A.S. Sofronov and P.G. Melnikov, The use of a thiadiazole derivative to inhibit mild steel corrosion in 1 M HCl solution: Electrochemical and surface active aspects, *Int. J. Corros. Scale Inhib*., 2023, **12**, no. 4, 2362–2374. doi: 10.17675/2305-6894-2023-12-4-48
39. K.F. Khaled and M.A. Amin, Computational and electrochemical investigation for corrosion inhibition of nickel in molar nitric acid by piperidines, *J. Appl. Electrochem*., 2008, **38**, no. 11, 1609–1621. doi: 10.1007/s10800-008-9604-5
40. A. Elgendy, H. Nady, M.M. El-Rabiei, A.A. Elhenawy, Understanding the adsorption performance of two glycine derivatives as novel and environmentally safe anti-corrosion agents for copper in chloride solutions: Experimental, DFT, and MC studies, *RSC Adv*., 2019, **9**, 42120–42131. doi: 10.1039/C9RA08617J

41. A. Visa, N. Plesu, B. Maranescu, G. Ilia, A. Borota and L. Crisan, Combined Experimental and Theoretical Insights into the Corrosion Inhibition Activity on Carbon Steel Iron of Phosphonic Acids, *Molecules*, 2021, **26**, 135. doi: 10.3390/molecules26010135
42. E.E. Ebenso, T. Arslan, F. Kandemirli, N. Caner and I. Love, Quantum chemical studies of some schiff bases as corrosion inhibitors for mild steel in acidic medium, *Int. J. Quantum Chem*., 2010, **110**, no. 5, 1003–1018. doi: 10.1002/qua.22306
43. C. Verma, E.E. Ebenso, M.A. Quraishi and I.B. Obot, Adsorption behavior of glucosamine-based, pyrimidine-fused heterocycles as effective corrosion inhibitors for mild steel in 1 M HCl: insights from electrochemical, thermodynamic and surface characterization studies, *J. Mol. Liq*., 2017, **236**, 139–148. doi: 10.1016/j.molliq.2017.03.085
44. I. Ahamad, R. Prasad and M.A. Quraishi, Inhibition of mild steel corrosion in acid solution by phenyl thiourea derivatives: electrochemical and thermodynamic study, *Corros. Sci*., 2010, **52**, no. 9, 3033–3041. doi: 10.1016/j.corsci.2010.05.022
45. K.F. Khaled and M.A. Amin, Corrosion monitoring of mild steel in sulphuric acid solutions in presence of some thiazole derivatives–molecular dynamics, chemical and electrochemical studies, *Corros. Sci*., 2009, **51**, no. 9, 1964–1975. doi: 10.1016/j.corsci.2009.05.002
46. A.S. Fouda, A.S. Ellithy and K. Shalabi, Some thiosemicarbazide derivatives as corrosion inhibitors for carbon steel in acidic solution, *Desalination*, 2009, **249**, no. 1, 1081–1090. doi: 10.1016/j.desal.2009.04.028

♦ ♦ ♦